

Nitrogen Chemisorption on the Coordinatively Unsaturated Rh Site on Al₂O₃

Edward A. Wovchko and John T. Yates, Jr.*

Contribution from the Surface Science Center, Department of Chemistry, University of Pittsburgh, Pittsburgh, Pennsylvania 15260

Received January 29, 1996[⊗]

Abstract: The UV (3.8 eV) photolysis of atomically-dispersed Rh^I(CO)₂ species supported on an Al₂O₃ surface in the presence of N₂ at 175 K caused the replacement of CO by N₂ ligands. Therefore dinitrogen chemisorption effectively probes the coordinatively unsaturated Rh(CO) species generated during photodecomposition of Rh^I(CO)₂/Al₂O₃. Two infrared bands, observed at 2234 and 2048 cm⁻¹, are attributed respectively to ν_{N₂} and ν_{CO} in Rh(N₂)(CO), and a band at 2188 cm⁻¹ is assigned to Rh(N₂)₂ surface species. The assignments are based on frequencies and the relative rates of spectral development for the two N₂-containing species. The Rh(N₂)₂ species on Al₂O₃ exhibits identical N–N stretching modes to a similar species produced by matrix isolation methods. It is shown that both the Rh–CO bond and the Rh–N₂ bond may be broken by photolysis.

1. Introduction

The ultraviolet photolysis of Rh^I(CO)₂ species, supported on Al₂O₃ (designated Rh^I(CO)₂/Al₂O₃), produces an unstable and coordinatively unsaturated Rh(CO) intermediate which can activate the C–H bond in alkanes^{1–4} and the H–H bond in hydrogen.⁵ The atomically-dispersed Rh^I(CO)₂ supported on Al₂O₃ is produced from disruption and oxidation of alumina-supported metallic Rh particles in a reaction with CO gas and surface hydroxyl groups.^{6–14} A critical step for successful bond activation in alkanes and in H₂ is the temporary adsorption of the molecule on the photochemically-generated Rh(CO) centers. For each of the above alkane and hydrogen bond activation studies, no direct observation of this temporarily existing intermediate was possible. In contrast, by photolyzing Rh^I(CO)₂ in the presence of nitrogen gas, we can successfully probe the photochemically generated Rh(CO) center by adsorbing N₂ to generate Rh(N₂)(CO) and Rh(N₂)₂ species.

There have been several infrared studies of N₂ adsorption on supported metal surfaces, such as Ni/SiO₂,¹⁵ Ru/Al₂O₃,¹⁶ Ru/MgO,¹⁶ and Pt/SiO₂.¹⁷ Only a few studies have involved the chemisorption of N₂ on supported Rh surfaces, and in these cases the infrared bands associated with adsorbed N₂ on metallic

Rh sites were of low intensity.^{18–22} Only recently have there been reports of a molecular complex of rhodium with mixed CO and N₂ ligands or two N₂ ligands.^{23,24} In several of the above mentioned studies, the molecular orientations of the adsorbed N₂ species were considered. Attempts were made to distinguish between two N₂ bonding possibilities—η¹-end-on bonding and η²-side-on bonding. In these instances, the exact type of bonding could not be determined.

In this paper, we have employed infrared spectroscopy and ultrahigh vacuum techniques to investigate the ultraviolet photolysis of Rh^I(CO)₂/Al₂O₃ in the presence nitrogen gas at 175 K. Nitrogen adsorption occurs on the photochemically generated Rh(CO) species, leading ultimately to the production of Rh(N₂)₂/Al₂O₃ species. Infrared spectra and Gaussian curve peak fitting were utilized to identify the Rh–N₂ species. Isotopic substitution experiments were conducted to examine the bonding orientation issues.

2. Experimental Section

All experiments were conducted in the special transmission infrared cell described in detail previously.^{25,26} The cell is a stainless steel cube with six conflat flange ports. Double viton O-ring-sealed, differentially-pumped KBr windows were attached to two of the ports for infrared beam transmission. A sapphire window was used for UV irradiation. Samples were spray deposited on a tungsten grid (0.0254 mm thick with 0.22 mm square openings exhibiting 70% optical transparency). The grid was secured by nickel clamps and mounted on electrical feedthroughs mounted on the bottom of a reentrant Dewar. The sample was heated electrically using a digital temperature programmer/controller²⁷ and cooled by filling the reentrant Dewar with liquid nitrogen. Sample temperatures were measured by a K-type thermo-

[⊗] Abstract published in *Advance ACS Abstracts*, October 1, 1996.
 (1) Ballinger, T. H.; Yates, J. T., Jr. *J. Am. Chem. Soc.* **1992**, *114*, 10074.
 (2) Ballinger, T. H.; Yates, J. T., Jr. *J. Phys. Chem.* **1992**, *96*, 9979.
 (3) Wong, J. C. S.; Yates, J. T., Jr. *J. Am. Chem. Soc.* **1994**, *116*, 1610.
 (4) Wong, J. C. S.; Yates, J. T., Jr. *J. Phys. Chem.* **1995**, *99*, 12640.
 (5) Wovchko, E. A.; Yates, J. T., Jr. *J. Am. Chem. Soc.* **1995**, *117*, 12557.
 (6) Yang, A. C.; Garland, C. W. *J. Phys. Chem.* **1957**, *61*, 1504.
 (7) Yates, J. T., Jr.; Duncan, T. M.; Worley, S. D.; Vaughan, R. W. *J. Chem. Phys.* **1979**, *70*, 1219.
 (8) Yates, J. T., Jr.; Duncan, T. M.; Vaughan, R. W. *J. Chem. Phys.* **1979**, *71*, 3908.
 (9) Cavanagh, R. R.; Yates, J. T., Jr. *J. Chem. Phys.* **1981**, *74*, 4150.
 (10) Yates, J. T., Jr.; Kolasinski, K. *J. Chem. Phys.* **1983**, *79*, 1026.
 (11) Rice, C. A.; Worley, S. D.; Curtis, C. W.; Guin, J. A.; Tarrer, A. *R. J. Chem. Phys.* **1981**, *74*, 6487.
 (12) Solymosi, F.; Pásztor, M. *J. Phys. Chem.* **1985**, *89*, 4789.
 (13) Basu, P.; Panayotov, D.; Yates, J. T., Jr. *J. Phys. Chem.* **1987**, *91*, 3133.
 (14) Basu, P.; Panayotov, D.; Yates, J. T., Jr. *J. Am. Chem. Soc.* **1988**, *110*, 2074.
 (15) Eischens, R. P.; Jacknow, J. *Proc. Int. Congr. Catal.* **1965**, *3*, 627.
 (16) Kubota, J.; Aika, K. *J. Phys. Chem.* **1994**, *98*, 11293.
 (17) Egerton, T. A.; Sheppard, N. *J. Chem. Soc., Faraday Trans. 1* **1974**, *70*, 1357.

(18) Borod'ko, Y. G.; Lyutov, V. S. *Kinet. Catal.* **1971**, *12*, 202.
 (19) Lyutov, V. S.; Fedosimov, V. A.; Borod'ko, Y. G. *Russ. J. Phys. Chem.* **1972**, *46*, 973.
 (20) Wang, H. P.; Yates, J. T., Jr. *J. Phys. Chem.* **1984**, *88*, 852.
 (21) Yates, J. T., Jr.; Haller, G. L. *J. Phys. Chem.* **1984**, *88*, 4660.
 (22) Pei, Z.; Fang, T. H.; Worley, S. D. *J. Phys. Chem.* **1995**, *99*, 3663.
 (23) Miessner, H. *J. Chem. Soc., Chem. Commun.* **1994**, 927.
 (24) Miessner, H. *J. Am. Chem. Soc.* **1994**, *116*, 11522.
 (25) Basu, P.; Ballinger, T. H.; Yates, J. T., Jr. *Rev. Sci. Instrum.* **1988**, *59*, 1321.
 (26) Wong, J. C. S.; Linsebigler, A.; Lu, G.; Fan, J.; Yates, J. T., Jr. *J. Phys. Chem.* **1995**, *99*, 335.
 (27) Muha, R. J.; Gates, S. M.; Yates, J. T., Jr.; Basu, P. *Rev. Sci. Instrum.* **1985**, *56*, 613.

couple spot welded on the top center of the tungsten grid. The temperature could be held constant and maintained to ± 2 K in the range 150 to 1500 K. The cell was flexibly connected to a bakeable stainless steel vacuum and gas delivery system. The system was pumped by 60 L s⁻¹ turbomolecular and 30 L s⁻¹ ion pumps achieving base pressures of $< 1 \times 10^{-8}$ Torr. The system was equipped with a Dycor M100M quadrupole mass spectrometer for gas analysis and leak checking. Gas pressures were measured with a MKS 116A Baratron capacitance manometer.

The 0.5% Rh/Al₂O₃ samples were prepared by dissolving RhCl₃·3H₂O (Alfa 99.9%) in ultrapure H₂O (10 mL/g of support). The solution was mixed with the appropriate amount of powdered Al₂O₃ (Degussa, 101 m²/g) and ultrasonically dispersed for approximately 45 min. This slurry was mixed with acetone (Mallinckrodt, AR) (9/1 acetone/H₂O volume ratio) and sprayed onto the tungsten grid using a nitrogen-gas pressured atomizer. The grid was warmed (~ 330 K) and spraying was interrupted intermittently to allow for solvent evaporation. The mixture was sprayed on a $\frac{2}{3}$ section (3.6 cm²) of the grid leaving a shielded $\frac{1}{3}$ (1.8 cm²) section clear for background scans. Deposits ranged from 25 to 34 mg (8.1 to 10.4 mg/cm²) depending on the spraying time.

Immediately after spraying, the sample was transferred to the infrared cell and evacuated at 475 K for 16–20 h. Following evacuation the sample was reduced at 475 K using four 190 Torr H₂ exposures at 15, 30, 45, and 60 min with evacuation after each exposure. The sample was evacuated at 475 K for another 18 to 20 h then cooled to 303 K and exposed to 5 Torr of CO for 10 min to convert the metallic Rh to Rh^I(CO)₂. The cell was evacuated and cooled to 172 K prior to nitrogen addition and photolysis experiments. The temperature never exceeded 179 K during each experiment (except for the photolysis of Rh^I(CO)₂ under vacuum (Figure 5, lower section) where the temperature was 200 K).

Infrared spectra were measured using a nitrogen-gas purged Mattson Research Series I Fourier transform infrared spectrometer equipped with a liquid nitrogen cooled HgCdTe wide band detector. Spectra were recorded by averaging 1000 or 1250 scans at 2 or 1 cm⁻¹ spectral resolution, respectively. The cell was translated laterally so the beam could pass through the unsprayed portion of the grid to obtain the background spectra. Small background features due to small deposits on the KBr windows were observed. Absorbance spectra were obtained by ratioing single beam spectra of the sample to background single beam spectra. All spectra were baseline corrected.

A 350-W high-pressure mercury-arc lamp provided the ultraviolet light for photolysis experiments. The optical bench was equipped with a f/1 two-element UV fused silica condensing lens, an iris diaphragm, and a shutter. The light was filtered by a 10 cm water infrared radiation filter and a 3.8 ± 0.5 eV (325 ± 50 nm) bandpass filter. Thermopile measurements indicate that the photofluxes of the filtered UV light were 7.4×10^{16} photons cm⁻² s⁻¹ $\pm 10\%$. Photochemistry and infrared measurements were conducted simultaneously without disturbing the position of the cell or UV lamp. This was done by orienting the UV light source perpendicular to the infrared beam. The tungsten grid was aligned in such a way that the infrared beam and the UV light were focused at a 45° angle to the normal of the grid.²⁶

Carbon monoxide (Matheson, 99.9%), ¹³C¹⁸O (Icon, 99% ¹³C, 95% ¹⁸O), ¹⁴N¹⁵N (Icon, 99% ¹⁵N), and ¹⁵N₂ (CIL, 98% ¹⁵N) were obtained in glass breakseal flasks and used without further purification. Hydrogen (Matheson, 99.9995%) and nitrogen (Matheson, 99.9999%) were obtained in steel cylinders and also used without further purification.

3. Results

3.1. Photolysis of Rh^I(CO)₂/Al₂O₃ in Nitrogen. The ultraviolet photolysis of Rh^I(CO)₂/Al₂O₃ in the presence of 185 Torr of nitrogen gas at 175 K is shown in Figure 1. The spectrum measured prior to any UV light exposure ($t_{UV} = 0$ min) contains a doublet at 2099 and 2028 cm⁻¹ characteristic of the symmetric and antisymmetric C–O stretching modes of the Rh^I(CO)₂ species generated by the oxidation and disruption of Rh crystallites during CO adsorption.^{6–14} After this spectrum was recorded, the shutter was opened allowing the sample to

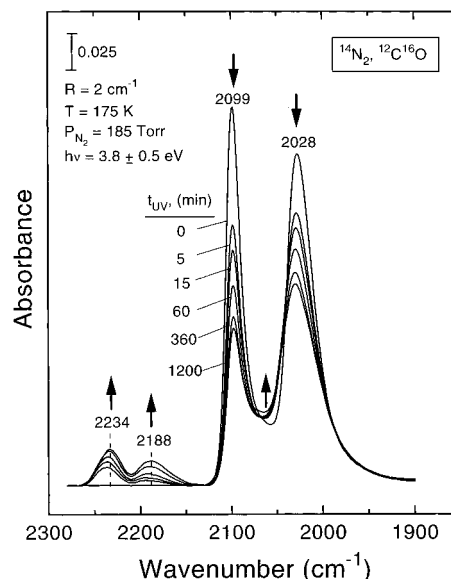


Figure 1. Infrared spectra measured in the N–N and C–O stretching regions during 1200 min of photolysis of Rh^I(CO)₂/Al₂O₃ in the presence of 185 Torr of N₂ at 175 K. The arrows indicate the direction of the absorbance changes.

be irradiated. Spectra were measured at various times during the 1200-min photolysis experiment revealing a continual decrease of the carbonyl bands at 2099 and 2028 cm⁻¹ (direction of development is indicated by the dark arrows). The decrease in the dicarbonyl bands is accompanied by the development of two bands centered at 2234 and 2188 cm⁻¹. These frequencies fall in the range for gaseous dinitrogen²⁸ and dinitrogen species adsorbed on single crystal and supported metal surfaces.^{15–24,29–33} Upon inspection, one can see that at earlier photolysis times (5 and 15 min) the band at 2234 cm⁻¹ grows at a faster rate than the 2188-cm⁻¹ band. The increase in intensity of the 2234-cm⁻¹ mode between 360 and 1200 min is much less than the increase of the 2188-cm⁻¹ mode during the last stages of the photolysis process. Both of these species were stable after evacuating the nitrogen gas at 175 K. A small intensity increase is also observed around 2048 cm⁻¹ between the two dicarbonyl bands at 2099 and 2028 cm⁻¹ as photolysis progresses. Bands in this region are typical for carbonyl species bonded in a terminal fashion to Rh centers.^{6–14}

The nitrogen features generated during the photolysis of Rh^I(CO)₂/Al₂O₃ can be removed both thermally and photochemically by an exchange process with CO. In Figure 2, spectrum a represents the surface after 1200 min of photolysis in the presence of nitrogen (from Figure 1). After the sample is exposed to 5 Torr of CO at 175 K for 60 min followed by evacuation, spectrum b is obtained. A partial loss of the 2234- and 2188-cm⁻¹ bands is observed along with an intensification of the dicarbonyl bands at 2099 and 2028 cm⁻¹. This thermal exchange rate slowed and the nitrogen species were then further removed by irradiating in the presence of 5 Torr of CO at 175 K (spectrum c). The dicarbonyl bands are regenerated back to

(28) Szymanski, H. S. *Raman Spectroscopy*; Plenum Press: New York/London, 1970; Vol. 2.

(29) Yoshinobu, J.; Zenobi, R.; Xu, J.; Xu, Z.; Yates, J. T., Jr. *J. Chem. Phys.* **1991**, *95*, 9393.

(30) Arumainayagam, C. R.; Tripa, C. E.; Xu, J.; Yates, J. T., Jr. *Surf. Sci.* **1996**, *360*, 121.

(31) Bandy, B. J.; Canning, N. D. S.; Hollins, P.; Pritchard, J. J. *J. Chem. Soc., Chem. Commun.* **1982**, 58.

(32) de Paola, R. A.; Hoffmann, F. M.; Heskett, D.; Plummer, E. W. *Phys. Rev. B* **1987**, *35*, 4236.

(33) Ho, W.; Willis, R. R.; Plummer, E. W. *Surf. Sci.* **1980**, *95*, 171.

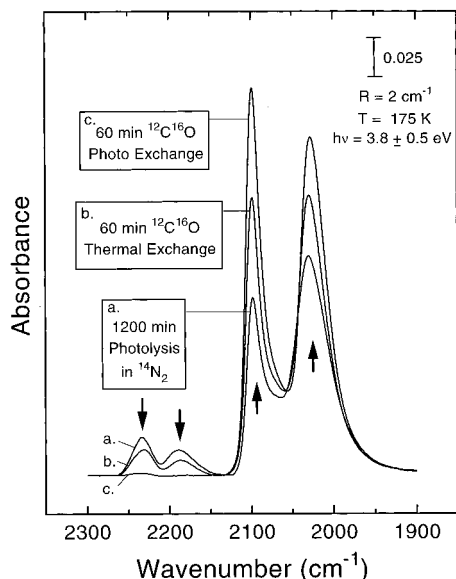


Figure 2. Thermal and photochemical exchange of $^{14}\text{N}_2$ surface species with $\text{CO}(\text{g})$ at 175 K. (a) Spectrum measured after 1200 min of photolysis of $\text{Rh}(\text{CO})_2$ in 185 Torr of nitrogen (from Figure 1). (b) Spectrum measured after evacuation of N_2 gas and exposure to 5 Torr of CO for 60 min at 175 K followed by evacuation. (c) Spectrum measured after photolyzing in 5 Torr of CO for 60 min followed by evacuation. The arrows indicate the direction of the absorbance changes.

their original intensity demonstrating the reversibility of the photoexchange process.

The adsorbed nitrogen also exchanges with itself upon irradiation. This is illustrated in Figure 3. Here, $^{13}\text{C}^{18}\text{O}$ was initially utilized to create isotopically labeled gem-dicarbonyl species, shifting the infrared bands appropriately to 2001 and 1940 cm^{-1} . The sample was then irradiated under 10 Torr of isotopically labeled $^{15}\text{N}_2$ at 175 K for 1200 min to produce the spectrum indicated at 0 min. Here two bands very similar in character to the bands generated using $^{14}\text{N}_2$ are observed around 2161 and 2117 cm^{-1} . Upon evacuation of $^{15}\text{N}_2$ and introduction of 10 Torr of $^{14}\text{N}_2$, virtually no exchange takes place thermally after 180 min at 175 K. However, after exposing the sample to UV light an immediate exchange takes place between adsorbed $^{15}\text{N}_2$ and gas-phase $^{14}\text{N}_2$. Both the high-frequency and low-frequency bands decrease in intensity for the $^{15}\text{N}_2$ modes and both increase in intensity for the $^{14}\text{N}_2$ modes. Complete replacement of $^{15}\text{N}_2$ species is achieved after 1200 min of irradiation. A slight decrease in carbonyl mode absorbance occurs during irradiation. This is consistent with the replacement of carbonyls by nitrogen as shown in Figure 1.

3.2. Absorbance Ratio of Nitrogen Infrared Bands. It can be seen in Figure 1 that the two nitrogen infrared bands developing during photolysis grow independently and at different rates. To inspect this in better detail, the peak absorbance of the 2234- and 2188-cm^{-1} features are plotted versus photolysis time in Figure 4. Formation of the high-frequency band occurs immediately and to a much greater fractional extent than the low-frequency band. It is not until the later stages of photolysis that the low-frequency band grows faster than the former. This effect is more clearly represented by the absorbance ratio of the 2188-cm^{-1} -band absorbance to the 2234-cm^{-1} -band absorbance. The absorbance ratio is small at the early photolysis times, and the ratio increases for increasing irradiation time. The absorbance of the low-frequency mode approaches that of the high-frequency mode for long irradiation times. This behavior indicates that the two infrared bands arise from two separate nitrogen-containing species.

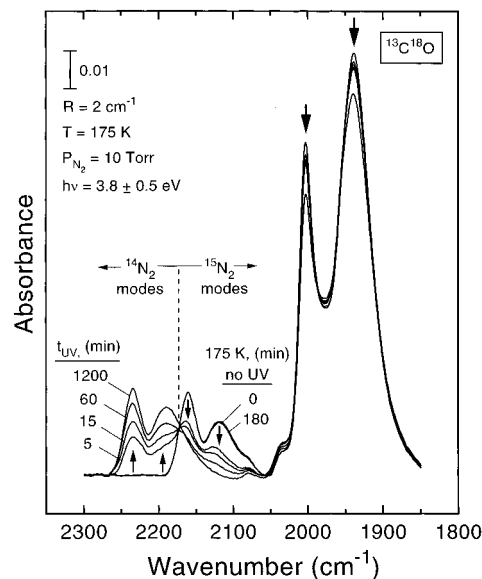


Figure 3. Photochemical exchange of isotopically labeled $^{15}\text{N}_2$ surface species with $^{14}\text{N}_2(\text{g})$ at 175 K. The spectrum to the right of the dashed line at 0 min represents 1200 min of photolysis of $\text{Rh}(^{13}\text{C}^{18}\text{O})_2/\text{Al}_2\text{O}_3$ in 10 Torr of $^{15}\text{N}_2(\text{g})$. The spectrum indicated at 180 min was measured in the presence of 10 Torr of $^{14}\text{N}_2$ after 180 min with no irradiation indicating that thermal exchange of N_2 ligands does not occur at 175 K. Spectra to the left of the dashed line represent spectra measured during irradiation in 10 Torr of $^{14}\text{N}_2$.

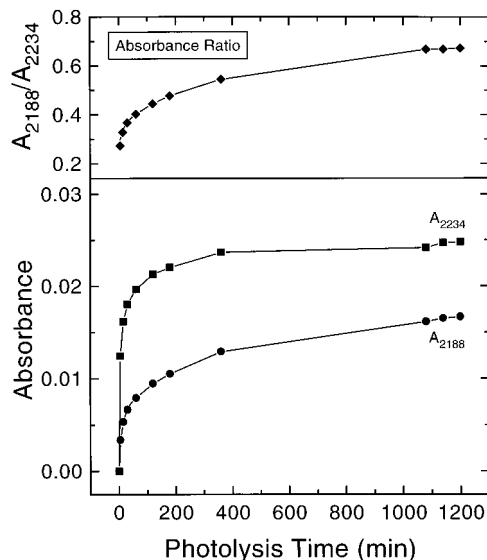


Figure 4. Sequential formation of N_2 infrared bands as a function of photolysis time. Absorbances of the 2234- and 2188-cm^{-1} bands are plotted in the lower portion. The absorbance ratio of the 2188-cm^{-1} band to the 2234-cm^{-1} band is plotted in the upper portion.

3.3. Developments in the Carbonyl Region during Photolysis. The gem-dicarbonyl infrared bands are lost during the UV photolysis of $\text{Rh}(\text{CO})_2/\text{Al}_2\text{O}_3$ in nitrogen. However, a small band near 2048 cm^{-1} was observed to grow between the two dicarbonyl bands in Figure 1 as irradiation took place. The difference spectrum measured after 360 min of irradiation in Figure 1 is displayed at the top of Figure 5. One can clearly see the two positive bands attributed to nitrogen species and also a positive feature at 2048 cm^{-1} (indicated by cross-hatching). The 2048-cm^{-1} feature is due to a carbonyl species as confirmed by a similar feature that develops at 1961 cm^{-1} when photolyzing isotopically labeled $\text{Rh}(^{13}\text{C}^{18}\text{O})_2/\text{Al}_2\text{O}_3$ in nitrogen.

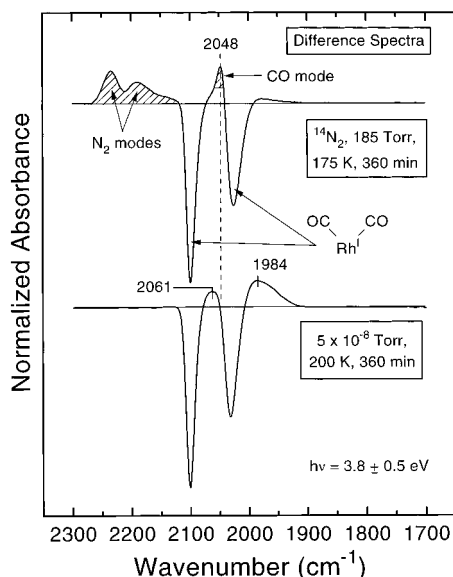


Figure 5. Infrared difference spectra of N₂ and CO modes during photolysis. The upper spectrum was measured after 360 min of irradiation in 185 Torr of N₂ at 175 K. The lower spectrum was measured after 360 min of irradiation at 5×10^{-8} Torr of N₂ at 200 K.

To more clearly understand the 2048-cm⁻¹ feature, an infrared difference spectrum of Rh^I(CO)₂/Al₂O₃ irradiated with UV light at 200 K in vacuum ($<5 \times 10^{-8}$ Torr) is shown in the lower portion of Figure 5. The spectrum has been normalized so that the loss of the 2099-cm⁻¹ symmetric dicarbonyl stretching mode matches the loss of the 2099-cm⁻¹ mode of the difference spectrum obtained for photolysis in N₂ as shown above. Photolysis of the dicarbonyl species under vacuum results in a similar loss of dicarbonyl bands, but positive features develop around 2061 and 1984 cm⁻¹. Assuming that the same contribution is present at 2061 cm⁻¹ for the photolysis under nitrogen case, there is still an additional contribution from a feature at 2048 cm⁻¹ (cross-hatched portion) that is not present in the vacuum experiment. This suggests the presence of a distinct carbonyl species in the nitrogen experiment. Also the magnitude of the band observed to develop at 1984 cm⁻¹ for the nitrogen experiment is much less than that observed in the vacuum experiment. The 1984-cm⁻¹ band is indicative of CO–Rh–Rh–CO species which do not form extensively in the presence of nitrogen during photolysis.

3.4. Curve Fit Analysis of Nitrogen Infrared Bands. The two nitrogen bands centered at 2234 and 2188 cm⁻¹ overlap with each other. At later stages of nitrogen uptake, the low-frequency band contributes somewhat to the high-frequency absorbance. The extent of contribution can be determined by fitting the experimental data to Gaussian curves. This is presented in Figure 6. Experimental data measured during a 1200-min UV irradiation of Rh^I(¹³C¹⁸O)₂/Al₂O₃ in 10 Torr of nitrogen are displayed in Figure 6A. A two-peak Gaussian curve fit of each spectrum in Figure 6A is shown in Figure 6B. The combination of the two fitted peaks for each spectrum is displayed in Figure 6C. One can visually see the close correlation between the combined fit (Figure 6C) and the original experimental data (Figure 6A). More importantly, the individual development of the high-frequency component (Figure 6B) increases in each sequential spectrum during the photolysis range and the plot of the relative absorbance of the 2188- and the 2234-cm⁻¹ features shown in the Gaussian fit curves strongly resembles the absorbance ratio measured directly from the experimental curves at the top of Figure 4. At no point does the intensity of the high-frequency component reach a maximum

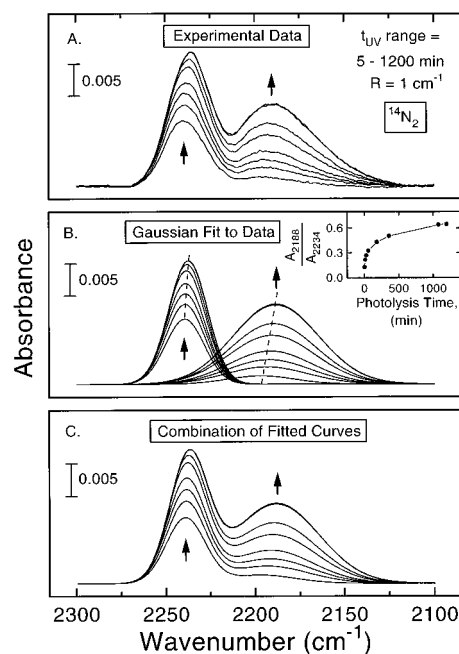


Figure 6. Curve fitting to experimental data for the N₂-region spectra. (A) Experimental spectra measured during 1200 min of photolysis in 10 Torr of N₂. (B) Two-peak Gaussian curve fit to experimental spectra in part A. (C) Combination of fitted Gaussian curves in part B.

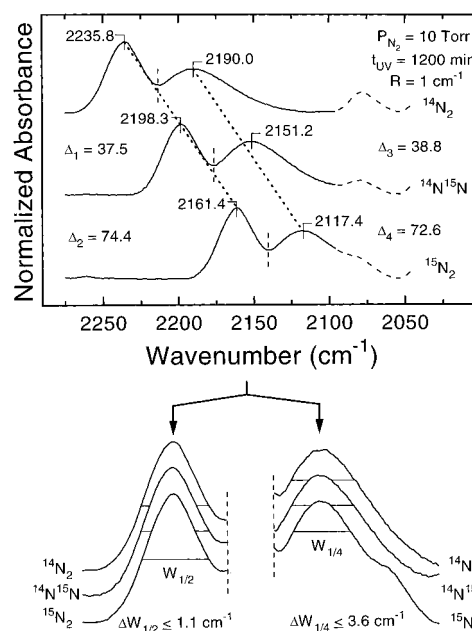


Figure 7. Nitrogen isotopic substitution effects. The upper section shows infrared spectra of separate samples measured after 1200 min of photolysis in 10 Torr of nitrogen for each isotope. The lower section represents the split, shifted, and normalized spectra from above.

and begin to decrease during the latter stages of photolysis. The low-frequency component also increases continually. This indicates that the two nitrogen-containing species are produced simultaneously and can mutually exist together. The 2234-cm⁻¹ band observed in Figure 6A does in fact grow at a decreasing rate throughout the entire irradiation experiment, as Rh^I(CO)₂ species are being consumed.

3.5. Nitrogen Isotopic Substitution Experiments—Halfwidth and Quarterwidth Analysis. The effect of nitrogen isotopic substitution during the UV photolysis of isotopically labeled Rh^I(¹³C¹⁸O)₂/Al₂O₃ is shown in Figure 7. Infrared spectra of the nitrogen stretching region measured after 1200 min of irradiation at 1-cm⁻¹ resolution for three separate samples can

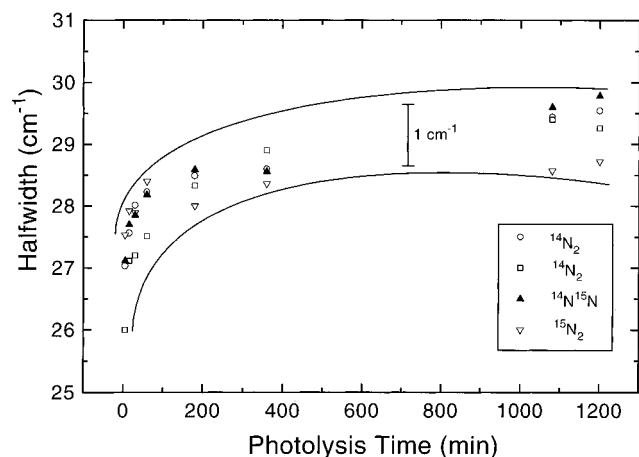


Figure 8. Halfwidth of the high-frequency nitrogen mode versus photolysis time for two $^{14}\text{N}_2$, one $^{14}\text{N}^{15}\text{N}$, and one $^{15}\text{N}_2$ experiment.

be seen for each nitrogen isotope. The dashed line portion of each spectrum (2090–2050 cm^{-1}) represents a small contribution from 5% $^{13}\text{C}^{16}\text{O}$ impurity in the isotopically labeled $^{13}\text{C}^{18}\text{O}$. Both nitrogen modes shift to lower frequency as one progresses from $^{14}\text{N}_2$ to $^{14}\text{N}^{15}\text{N}$ to $^{15}\text{N}_2$. Within the experimental frequency accuracy, one can see that both N_2 bands shift in a parallel fashion as the isotopic composition of the N_2 is changed.

In the lower portion of Figure 7, the spectra from above were shifted, normalized, and separated for purposes of illustrating the line width behavior for the different isotopic versions of the same surface species. The full width at half maximum ($W_{1/2}$) is indicated for the high-frequency mode, and the full width at quarter maximum ($W_{1/4}$) is drawn for the low-frequency mode for each isotope. The maximum change in halfwidth for the high-frequency mode is less than 1.1 cm^{-1} and the maximum change in quarterwidth for the low-frequency mode is less than 3.6 cm^{-1} , for the various isotopic species.

In Figure 8, the halfwidth of the high-frequency nitrogen mode is plotted as a function of photolysis time for two $^{14}\text{N}_2$ experiments, and for one $^{14}\text{N}^{15}\text{N}$ and one $^{15}\text{N}_2$ experiment. One can see that the range of halfwidths measured for a given photolysis time is 0.5–1.5 cm^{-1} with an overall average halfwidth difference of 0.9 cm^{-1} (from eight time measurements) independent of which isotopic N_2 species was used. In Figure 7, the maximum difference between quarterwidths of the low-frequency mode was 3.6 cm^{-1} . The influence of the absorbance due to $^{13}\text{C}^{16}\text{O}$ impurity is more significant for the quarterwidth for both the $^{14}\text{N}^{15}\text{N}$ and $^{15}\text{N}_2$ at short photolysis times. Because of this, a comparison for the low-frequency mode is not presented.

4. Discussion

4.1. Photochemistry of $\text{Rh}^{\text{I}}(\text{CO})_2/\text{Al}_2\text{O}_3$ in Nitrogen.

Irradiation of $\text{Rh}^{\text{I}}(\text{CO})_2/\text{Al}_2\text{O}_3$ causes the desorption of CO to produce the coordinatively unsaturated $\text{Rh}(\text{CO})/\text{Al}_2\text{O}_3$ species. This species provides an active site for the dissociation of the C–H bond in alkanes^{1–4} and the H–H bond in H_2 .⁵ For $\text{Rh}^{\text{I}}(\text{CO})_2$ photolysis in the presence of $\text{N}_2(\text{g})$, the N_2 species are adsorbed on the coordinatively unsaturated Rh sites, but N–N bond scission does not occur. This is a reasonable consequence of the isoelectronic nature of N_2 and CO.

The N–N stretching mode for $^{14}\text{N}_2(\text{g})$ is at 2331 cm^{-1} .²⁸ N_2 chemisorbed on metallic surfaces exhibits a lower N–N stretching frequency in a 200- cm^{-1} range below that of $\text{N}_2(\text{g})$. The two infrared frequencies observed for $^{14}\text{N}_2$ in this work at 2234 and 2188 cm^{-1} fall within the range of chemisorbed N_2 , but not of N_2 physisorbed on Al_2O_3 , which exhibits an N–N

stretching frequency near 2331 cm^{-1} .^{20,21,34} The two bands at 2234 and 2188 cm^{-1} differ from the frequency measured for N_2 chemisorption on metallic Rh sites which was at 2258²⁰ or 2248 cm^{-1} .²² N_2 adsorption on metallic Rh sites produces N–N absorption bands which are much weaker than the bands observed in this work.^{20,22}

4.2. Identification of the Two Nitrogen Species. Based on what is known about the photolysis of $\text{Rh}^{\text{I}}(\text{CO})_2/\text{Al}_2\text{O}_3$ ^{1–5} and the reversibility of carbonyl and nitrogen exchange during photolysis (Figure 1–3), the most logical species generated during irradiation in nitrogen gas are indicated in the following reaction sequence:



The photolysis of $\text{Rh}^{\text{I}}(\text{CO})_2/\text{Al}_2\text{O}_3$ results in the loss of a carbonyl ligand and the subsequent adsorption of N_2 to form a $\text{Rh}(\text{N}_2)(\text{CO})$ species. An additional loss of the second carbonyl ligand leads to the formation of a $\text{Rh}(\text{N}_2)_2$ species. The $\text{Rh}(\text{N}_2)(\text{CO})$ species would be expected to exhibit infrared bands in the N_2 and CO stretching regions. The $\text{Rh}(\text{N}_2)_2$ would only display infrared band(s) in the N_2 stretching region. Since the high-frequency mode at 2234 cm^{-1} is predominately formed at the early stages of photolysis, it will be assigned to $\text{Rh}(\text{N}_2)(\text{CO})$ and the 2188- cm^{-1} mode, which develops fully only at later stages, will be assigned to $\text{Rh}(\text{N}_2)_2$. This is consistent with reaction sequence 1. An alternate assignment of the 2234- and 2188- cm^{-1} bands to symmetric and antisymmetric coupled modes for $\text{Rh}(\text{N}_2)_2$ is inconsistent with the changing absorbance ratio for these two bands as photolysis takes place as shown in Figure 4. The changing absorbance ratio differs from the unchanging ratio observed during the formation of $\text{Rh}^{\text{I}}(\text{CO})_2$.⁷

A carbonyl feature at 2048 cm^{-1} develops during photolysis in Figure 1. This spectral band is more clearly seen in the difference spectrum displayed in Figure 5. The actual intensity of the 2048- cm^{-1} band may be attenuated on its low-frequency edge by the strong negative difference feature at 2028 cm^{-1} caused by depopulation of the dicarbonyl species. The 2048- cm^{-1} band is superimposed on a positive feature at 2061 cm^{-1} which is observed as a singular feature in this spectral region for photolysis experiments in vacuum (bottom of Figure 5). We assign the 2048- cm^{-1} mode to $\text{Rh}(\text{N}_2)(\text{CO})$ and the 2061- cm^{-1} mode to coordinatively unsaturated $\text{Rh}(\text{CO})$. The assignment of the 2048- cm^{-1} mode to $\text{Rh}(\text{N}_2)(\text{CO})$ is consistent with other assignments, for example $\text{Rh}(\text{H})(\text{CO})$ at 2020–2045 cm^{-1} .^{35–38}

A second feature which is prominent in the photolysis experiment in vacuum is the 1984- cm^{-1} band. This band is not strongly observed when $\text{Rh}^{\text{I}}(\text{CO})_2$ photolysis occurs under $\text{N}_2(\text{g})$. It is possible that it is due to CO–Rh–Rh–CO species which preferentially form by dimerization of photochemically produced $\text{Rh}(\text{CO})$ species when N_2 is unavailable to bond to the coordinatively unsaturated site.

The assignment of $\text{Rh}(\text{N}_2)_2$ at 2188 cm^{-1} is in excellent agreement with 10 K matrix isolation experiments involving the co-condensation of Rh atoms with N_2 to form $\text{Rh}(\text{N}_2)_n$ with $n = 1–4$.³⁹ In that work, a single band measured at 2188 cm^{-1} was assigned to $\text{Rh}(\text{N}_2)_2$ species, in exact agreement with our band at 2188 cm^{-1} . For isotopically labeled $\text{Rh}(^{15}\text{N}_2)_2$, the band

(34) Neyman, K. M.; Strodel, P.; Ruzankin, S. P.; Schlenz, N.; Knözinger, H.; Rösch, N. *Catal. Lett.* **1995**, *31*, 273.

(35) Henderson, M. A.; Worley, S. D. *J. Phys. Chem.* **1985**, *89*, 1417.

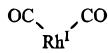
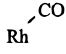
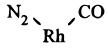
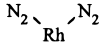
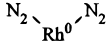
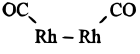
(36) McKee, M. L.; Dai, C. H.; Worley, S. D. *J. Phys. Chem.* **1988**, *92*, 1056.

(37) Solymosi, F.; Pásztor, M. *J. Catal.* **1987**, *104*, 312.

(38) Solymosi, F.; Knözinger, H. *J. Chem. Soc., Faraday Trans.* **1990**, *86*, 389.

(39) Ozin, G. A.; Voet, A. V. *Can. J. Chem.* **1973**, *51*, 3332.

Table 1. Spectroscopic Assignment of Surface Species

Species	ν_{CO} (cm ⁻¹)	ν_{N_2} (cm ⁻¹)	Ref.
	2099 2028	-	This work and many others [6-14]
	2061	-	This work
	2048	2234	This work
	-	2188	This work
	-	2188	[39]
	1984	-	This work

shifted to 2113 cm⁻¹,³⁹ in good agreement with our isotopically shifted band for Rh(¹⁵N)₂ at 2117 cm⁻¹. The matrix isolation Rh(N₂)_n species produced infrared bands displaying halfwidths of only 1–2 cm⁻¹, compared to halfwidths of 27–30 cm⁻¹ for Rh(N₂)(CO)/Al₂O₃ and quarterwidths of 27–34 cm⁻¹ for Rh(N₂)₂/Al₂O₃ in this work. It should be noted that the matrix isolation experiments were done with Rh⁰ atom deposits, whereas our studies involve Rh centers whose oxidation number cannot be determined in this work.

Table 1 shows the spectroscopic assignments of all the species observed in this work.

The possibility that Rh–OCN and/or Rh–NCO species are generated during the photolysis can be eliminated based on the results of our isotopic substitution experiments. In Figure 7, where Rh(¹³C¹⁸O)₂ was initially produced prior to photolysis, the 2236- and 2190-cm⁻¹ infrared bands for ¹⁴N₂ are nearly identical to the bands observed in Figure 1, where Rh(¹²C¹⁶O)₂ was initially present. These bands at 2236 and 2190 cm⁻¹ are much too high in frequency for potential Rh–¹⁸O¹³CN and Rh–¹³C¹⁸O species, respectively.⁴⁰

A study involving high-temperature (523 K) CO, H₂, and N₂ flow experiments on Rh supported on dealuminated Y zeolite surface was reported recently by Miessner.²⁴ Several infrared bands were observed in both the nitrogen and the carbonyl stretching regions. He assigned a 2060-cm⁻¹ carbonyl band and a band at 2251 cm⁻¹ in the N₂ region to Rh(CO)(N₂) species. The nitrogen species were only stable at high nitrogen pressure under flowing conditions. Although the CO and N₂ frequencies are somewhat higher, the assignment is similar to this study. These differences may be due to preparation procedure differences or to large temperature differences in the spectroscopic measurements.

4.3. Production of the Two Species Involving N₂. According to reaction sequence 1, the production of Rh(N₂)₂ depends first upon the formation of Rh(N₂)(CO). The detailed development of the two N–N stretching modes for the two

Table 2. Predicted N–N Stretching Frequencies for Both Rh¹⁴N¹⁵N and Rh¹⁵N¹⁴N Species Using an Unsymmetric Triatomic Linear Oscillator Model⁴⁹ and Assuming a Rh–N Stretching Frequency of 345 cm⁻¹³⁹

		$k_1 \quad k_2$		Rh–N=N	
k_1 , N m ⁻¹	k_2 , N m ⁻¹	$\nu_{\text{N-N}}(^{14}\text{N}^{15}\text{N})$, cm ⁻¹	$\nu_{\text{N-N}}(^{15}\text{N}^{14}\text{N})$, cm ⁻¹	$\Delta\nu_{\text{N-N}}$, cm ⁻¹	
100	2000	2169.0	2167.2	1.8	
150	2000	2184.8	2182.1	2.7	
200	2000	2200.5	2196.9	3.6	
250	2000	2216.1	2211.6	4.5	
300	2000	2231.6	2226.2	5.4	
350	2000	2247.0	2240.7	6.3	
400	2000	2262.2	2255.1	7.1	
450	2000	2277.4	2269.4	8.0	
500	2000	2292.5	2283.6	8.9	

species is best seen in the Gaussian fits shown in Figure 6, where it is seen that the rate of development of the 2234-cm⁻¹ band assigned to Rh(N₂)(CO) continually decreases as the Rh(N₂)₂ band at 2188 cm⁻¹ develops. This behavior is in accordance with the sequential photochemical development of Rh(N₂)₂ by way of the intermediate species Rh(N₂)(CO), although the consumption of Rh(N₂)(CO) was not observed even after 1200 min of photolysis. Even though the intermediate species Rh(N₂)(CO) is being consumed to produce Rh(N₂)₂, it is also being reformed from Rh^I(CO)₂ throughout the entire 1200-min experiment.

Both of the N₂ stretching modes for Rh(N₂)(CO) and Rh(N₂)₂ shift slightly to lower frequency as the intensity and surface coverage increases (Figure 6B). This may be due to inhomogeneities in the Al₂O₃ sites which bind the Rh centers.

4.4. Nitrogen-Bonding Issues. The question of molecular orientation of N₂ in the M–N₂ moiety (M = Mo, Ni, Ru, Rh, W, and V, for example) has been an issue for numerous organometallic complexes with dinitrogen^{41–46} and for some surface studies.^{15,20,47} The issue is whether the dinitrogen ligand is bonded by an η^1 -end-on configuration, involving primarily σ bonding between the metal center and only 1 nitrogen atom, or η^2 -side-on type bonding, in which the bonding occurs through the π bonds between both nitrogen atoms. Examples of both bonding types are found in the literature,^{41–46} but end-on bonding is much more prevalent. Molecular orbital studies of RhCl(PH₃)₂(N₂) indicate that end-on bonding is more stable. This is because the Rh center receives much larger electrostatic stabilization as a result of slightly larger N₂ donation from η^1 -N₂ bonding than from η^2 -N₂ bonding.⁴⁸ In principle, end-on bonded Rh–N₂ species would be spectroscopically distinguishable from side-on Rh–N₂ when isotopically labeled ¹⁴N¹⁵N is the ligand. A splitting of the infrared band is expected due to the formation of two species, Rh¹⁴N¹⁵N and Rh¹⁵N¹⁴N, in the end-on bonded Rh–N₂. Table 2 shows the predicted N–N stretching frequency ($\nu_{\text{N-N}}$) for both Rh¹⁴N¹⁵N and Rh¹⁵N¹⁴N

(41) Chatt, J.; Dilworth, J. R.; Richards, R. L. *Chem. Rev.* **1978**, *78*, 589.

(42) Hidai, M.; Mizobe, Y. *Chem. Rev.* **1995**, *95*, 1115.

(43) Gambarotta, S. *J. Organomet. Chem.* **1995**, *500*, 117.

(44) Busetto, C.; D'Alfonso, A.; Maspero, F.; Perego, G.; Zazzetta, A. *J. Chem. Soc., Dalton Trans.* **1977**, 1828.

(45) Thorn, D. L.; Tulip, T. H.; Ibers, J. A. *J. Chem. Soc., Dalton Trans.* **1979**, 2022.

(46) Ozaki, A.; Aika, K. In *Catalysis-Science and Technology*; Anderson, J. R., Boudart, M., Eds.; Springer Verlag: New York, 1981; Vol. 1, Chapter 3.

(47) Fang, T. H.; McKee, M. L.; Worley, S. D. *Can. J. Chem.* **1994**, *72*, 519.

(48) Sakaki, S.; Morokuma, K.; Ohkubo, K. *J. Am. Chem. Soc.* **1985**, *107*, 2686.

(40) Paul, D. K.; McKee, M. L.; Worley, S. D.; Hoffman, N. W.; Ash, D. H.; Gautney, J. J. *Phys. Chem.* **1989**, *93*, 4598.

species using a simple unsymmetric triatomic linear oscillator model.⁴⁹ Frequencies were calculated over a range of possible Rh–N force constants (k_1), assuming a N–N force constant of 2000 N m⁻¹ (k_2) and a Rh–N stretching frequency of 345 cm⁻¹ (the observed infrared frequency is in ref 39). The change in frequencies ($\Delta\nu_{\text{N-N}}$) spans from 1.8 to 8.9 cm⁻¹ over the range of Rh–N force constants. The expected frequency difference is 3.6 cm⁻¹ for the frequency closest to the observed ¹⁴N–¹⁵N frequency of 2198 cm⁻¹, according to this model, as may be seen by inspection of Table 2. In the Rh atom/N₂ co-condensation matrix isolation studies,³⁹ band splitting (1.7 cm⁻¹) was observed for Rh–¹⁴N¹⁵N and Rh–¹⁵N¹⁴N species, unequivocally proving end-on bonding. These bands were very sharp, displaying halfwidths of ~1–2 cm⁻¹ (as opposed to ~30 cm⁻¹ halfwidths measured here).

The average halfwidth difference for the ¹⁴N₂-, ¹⁴N¹⁵N-, and ¹⁵N₂-containing species was 0.9 cm⁻¹ measured at various photolysis times up to 1200 min (Figure 8). For the expected frequency shift of the two Rh–¹⁴N¹⁵N and Rh–¹⁵N¹⁴N species [1.7 cm⁻¹ (ref 39) to 3.6 cm⁻¹ (model)], the superposition of broadened and shifted Gaussians (30-cm⁻¹ halfwidth) would yield an experimental broadening of ≤0.7 cm⁻¹ which would be unobservable in our experiments. Therefore we cannot distinguish η^1 -N₂ bonding from η^2 -N₂ bonding.

For the species Rh(N₂)₂, antisymmetric and symmetric vibrational coupling effects between the two N₂ moieties would be expected. Although the width of the spectral transition for Rh(N₂)₂ exceeds that for the Rh(N₂)(CO) species, no splitting is evident. This indicates that vibrational coupling is smaller between N₂ ligands than between CO ligands in the Rh(N₂)₂ species compared to Rh^I(CO)₂ species. The bandshape of the 2234-cm⁻¹ Rh(N₂)(CO) band remains essentially constant ($\Delta W_{1/2} = 1.4$) throughout the 1200-min photolysis in Figure 1. This constant halfwidth also eliminates the possibility of a Rh(N₂)₂ coupling component overlapping with the Rh(N₂)(CO) band.

The difference in the infrared band frequency (2234 and 2188 cm⁻¹) for the two dinitrogen species may be explained by the relative π interactions of the N₂ and CO ligands. Considering η^1 -end-on N₂ bonding for both Rh(N₂)₂ and Rh(N₂)(CO) species, both N₂ and CO ligands provide σ donation and both are regarded as π acceptors with N₂ being a weaker π acceptor than CO.⁴¹ For the Rh(N₂)₂ species, both N₂ ligands are required to equally distribute Rh d π orbital electron density into their

π^* antibonding orbitals. This backbonding leads to a strengthening of the Rh–N bond and weakening of the N–N bond thus lowering the N–N stretching frequency.^{41,50,51} For the Rh(N₂)(CO) species, the stronger bonding CO ligand would extract a greater percentage of electron density from the Rh d π orbitals into its π^* orbitals than the N₂ ligand. In this case, the N–N bond would not be weakened to the extent of the N–N bond in Rh(N₂)₂ species and thus have a higher N–N stretching frequency. This supports the assignment of the 2234-cm⁻¹ N₂ band to Rh(N₂)(CO) and the 2188-cm⁻¹ N₂ band to Rh(N₂)₂.

5. Conclusions

The following conclusions can be made about the ultraviolet irradiation of Rh^I(CO)₂/Al₂O₃ in the presence of nitrogen gas at 175 K.

(1) Molecular nitrogen adsorbs on the photochemically-generated coordinatively unsaturated Rh(CO) center. Infrared bands which develop at 2234 and 2048 cm⁻¹ are attributed to the N₂- and CO-respective stretching modes of Rh(N₂)(CO) and a band at 2188 cm⁻¹ is assigned to the N₂ stretching mode of Rh(N₂)₂.

(2) The Rh(N₂)(CO) species is initially produced and is an intermediate surface species for the formation of Rh(N₂)₂ species by continued photolysis.

(3) Both Rh(N₂)(CO) and Rh(N₂)₂ surface species are able to be photoexcited, and N₂ and CO photodesorption occurs from these excited surface species, leading to (a) CO replacement by isotopic CO, (b) CO replacement by N₂, (c) N₂ replacement by isotopic N₂, and (d) N₂ replacement by CO.

(4) Isotopic substitution experiments to discriminate η^1 -N₂ and η^2 -N₂ species in Rh(N₂)(CO) were unsuccessful. However, based on exact N–N frequency agreement with matrix isolation experiments for Rh(N₂)₂, in which η^1 -bonding occurs, it is likely that the Rh(N₂)(CO) species also involves η^1 -N₂ bonding.

(5) This work, through the stabilization and observation of the Rh(N₂)(CO) species, is the first spectroscopic study of the bonding of a molecule to the coordinatively unsaturated Rh site in Rh(CO)/Al₂O₃ preparations.

Acknowledgment. We thank the Department of Energy, Office of Basic Energy Sciences for support of this work. We also thank Professor N. John Cooper from the University of Pittsburgh for helpful discussions.

JA960303M

(50) Huheey, J. E. *Inorganic Chemistry: Principles of Structure and Reactivity*, 3rd ed.; Harper & Row: New York, 1983; Chapter 9.

(51) Butler, I. S.; Harrod, J. F. *Inorganic Chemistry: Principles and Applications*; Benjamin/Cummings: Redwood City, CA, 1989; Chapter 22.

(49) Herzberg, G. *Molecular Spectra and Molecular Structure II*, 7th ed.; D. Van Nostrand Co.: Princeton, NJ, 1956; pp 173–174.